Electronic Supplementary Material (ESI) for Lab on a Chip.

Electronic Supplementary Information

Splitting and separation of colloidal streams in sinusoidal microchannels

Mathias Schlenk[a], Markus Drechsler[a,b], Matthias Karg[c], Walter Zimmermann[d], Martin Trebbin[e,*], Stephan Förster[a,f,*]

[a] Physical Chemistry I, University of Bayreuth, 95440 Bayreuth, Germany.

[b] Bavarian Polymer Institute, University of Bayreuth, 95440 Bayreuth, Germany.

[c] Physical Chemistry I, Heinrich-Heine-University, 40204 Düsseldorf, Germany.

[d] Theoretical Physics I, University of Bayreuth, 95440 Bayreuth, Germany.

[e] Centre for Ultrafast Imaging (CUI), University of Hamburg, 22761 Hamburg, Germany.

[f] JCNS-1/ICS-1, Forschungszentrum Jülich, 52428 Jülich, Germany

Corresponding Authors:

Stephan Förster

JCNS-1/ICS-1, Forschungszentrum Jülich, D-52428 Jülich, Germany

Phone: +49 2461 61 85161, Fax: +49 2461 61 2610,

Email: s.foerster@fz-juelich.de

Martin Trebbin

Centre for Ultrafast Imaging, University of Hamburg, D-22761 Hamburg, Germany

Phone: +49 40 8998 2613

Email: martin.trebbin@uni-hamburg.de

Detailed photo- and soft lithographical microchip fabrication

The whole preparation process of polydimethylsiloxane (PDMS) microfluidic devices is shown in Fig. S1. The first step contains the photolithography which is performed in a clean room by spin-coating (Cee 200X, Brewer Science Inc.) a negative photoresist (SU-8 50, Microchem Corp.) onto a 3" silicon wafer, as visible in Fig. S1A. If a so-called 2D-chip design for 2D-focusing is prepared, just one layer of photo resist SU8-50 is spin-coated to build up a channel structure of 100 µm height. For producing a 3D-focusing chip design, two layers about 50 µm and 100 µm as well as two chip parts with channel structures are necessary to finally receive a higher channel height for the two side channels of 250 µm in comparison to the middle channel with 50 µm. The microchannel structures are imparted to the photoresist using a mask aligner (MJB4, SÜSS MicroTec SE). The uncured photoresist is removed in the subsequent development process which yields a one-layered respectively two-layered master. All detailed geometric design parameters of the sinusoidal and linear microchannels are shown in the main publication. The second part of the fabrication process, the soft lithography[1] , continues under dust-free conditions by replicating the micro structured master using polydimethylsiloxane (PDMS, Sylgard 184 kit, Dow Corning Corp.) and curing it for t = 1.5 h at T = 75 °C, as visible in Fig. S1B. The PDMS replica is removed from the master and inlet ports are punched into the polymer using home-made punch needles with an outer diameter of d = 1 mm. The PDMS is cut into smaller pieces for better handling whereby the channel design allows preparing several microchannels simultaneously. The final microfluidic device is created by bonding the PDMS replica for a 2D-chip onto a glass slide and the two structured PDMS chip halves to each other for a 3D-device. This is achieved by activating the PDMS and glass surface using air plasma (MiniFlecto-PC-MFC, Gala Instrumente GmbH), respectively the two PDMS chip halves by adding a little drop of pure water (0.2 µm-filtered Millipore) for initially aligning and finally drying at T = 30 °C for about t = 1 h. The use of a microscope helps during the alignment step and in addition to it the integrated orientation structures of the multi-layer design will snap in and align the microstructures automatically with high precision.

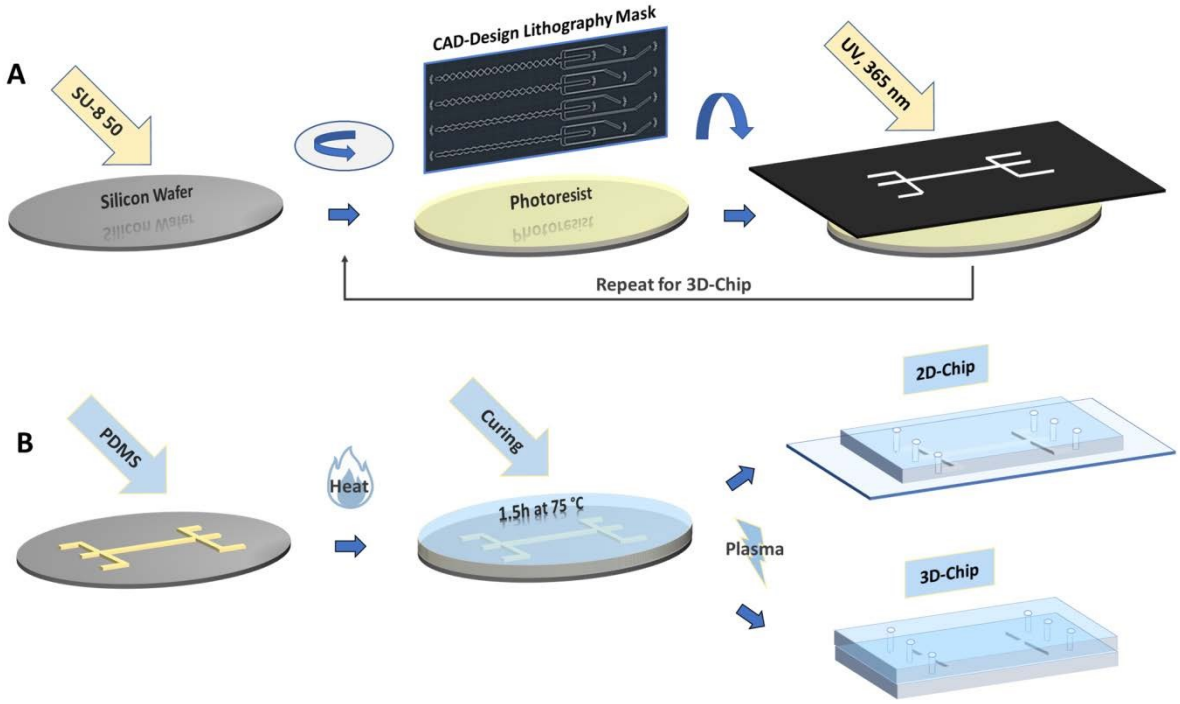

Fig. S1 Fabrication of microfluidic devices made of PDMS. (A) Master device fabrication based on SU-8 50 photoresist using photolithography with UV-exposure whereby the photolithographic master for 3D-chips involves one repeating step to build up a multilayered microstructure. After development, the uncured photoresist is removed. (B) The resulting 2D- respectively 3D-microchannel template is replicated by using soft lithography[1]. Therefore, the PDMS is poured onto the master device and cured for $t = 1.5$ h at $T = 75$ °C. Afterwards, the PDMS replica is peeled off the master device, cut into the chip parts and inlet ports for fluids are added. After plasma treatment of the two PDMS halves respectively the glass surface for a 2D-chip, the device is sealed using air plasma treatment.

Characterization of colloids

The microfluidic devices for detailed jet-splitting analysis have been run by focused wormlike micelles which are prepared out of polyisoprene-*b*-polyethylene oxide (PI-PEO) and are polydisperse concerning their length. A solution with a concentration of c = 0.1 wt% wormlike micelles is shown by a cryo-transmission electron microscopy (cryo-TEM) image in Fig. S2A. The 2D-microfluidic chips with sinusoidal microchannels have been used to carry out separation experiments on a mixture of two different sizes of silica-poly-*N*-isopropyl-acrylamide (SiO_2-PNIPAM) core-shell particles. The mixture consisted of SiO_2-PNIPAM core-shell particles with a diameter of d = 600 nm (polydispersity index, PDI = 0.03) labeled with rhodamine B respectively 1000 nm (PDI = 0.25) labeled with fluorescein. A sample of the bigger core-shell particles with a diameter of 1000 nm is visible by fluorescent microscopy in Fig. S2B and the sample of the smaller particles with a diameter of 600 nm are shown in the fluorescent microscopic (FlucMic) image of Fig. S2C. The separation experiments have been run by using a 2D-microfluidic chip with sinusoidal microchannels as well as lateral focusing by the side channels via a non-Newtonian solution of polyethylene glycol (PEG) in water. A sample of 1 wt% PEG with a molar mass of M = 900,000 g/mol which includes the bimodal size distributed mixture of 600 nm and 1000 nm core-shell particles are displayed by the scanning electron microscopy (SEM) image of Fig. S2D. Here, the prepared sample was dried out at a certain percentage before SEM images could be taken which led to a recrystallization of the polyethylene glycol polymer chains. Thus, bundles of PEG chains could be observed via SEM which verified the expected PEG polymer network.

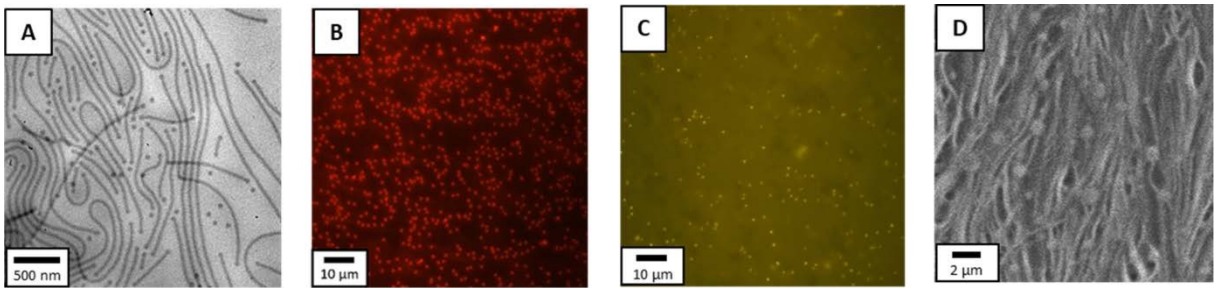

Fig. S2 (A) Cryo-TEM image of a PI_{110}-PEO_{198} wormlike micelles solution with a concentration of c = 0.1 wt% in water. (B) FlucMic image of rhodamine B-labeled SiO_2-PNIPAM core-shell particles with a total diameter of 1000 nm and a concentration of c = 0.17 vol% in water. (C) FlucMic image of fluorescein-labeled SiO_2-PNIPAM core-shell particles with a total diameter of 600 nm and a concentration of c = 0.13 vol% in water. (D) SEM image of a sample of 1 wt% PEG with a molar mass of M = 900,000 g/mol including the bimodal size distributed mixture of 600 nm and 1000 nm core-shell particles.

Detailed flow profile analysis

In all three parts of Fig. S3 are shown 3-dimensional confocal laser scanning microscopy (3D-CLSM) images for flow profile analysis of focused wormlike micelles (1 wt%) flowing in a sinusoidal microchannel with a width of w = 250 µm, a height of h = 100 µm and a distance of L = 15 mm as well as a periodic wavelength of P = 800 µm and an amplitude of A = 150 µm. In Fig. S3A, a mixture of 1 wt% wormlike micelles dyed with Nile red and 1 wt% PEG with a molar mass of 900,000 g/mol in water was pumped in one inlet through a sinusoidal microfluidic channel of a 2D-chip with varying flow rates. The images for flow rates of v = 30 µL/h, 200 µL/h and 2000 µL/h concerning each of the three inlets show no appearing jet-splitting effect if no colloid focusing by a cross section with side channels is used. Thus, a 2D-device with lateral 2D-focusing of the 1 wt% wormlike micelle solution via non-Newtonian 1 wt% PEG (M = 900,000 g/mol) from the two side channels is shown in Fig. S3B for a flow rate of v = 80 µL/h for all three inlets. Here, the jet-splitting effect has developed in one main stream and two horizontally divided sub-streams by using the contact of the shear thinning wormlike micelle solution to the top and bottom of the microchannel at the beginning cross section where the highest shear rates appear. As visible, the jet-splitting increases with each sine wave due to the existing expansion zones with higher extension rates after each narrowing section which leads to a shear thinning and sideward pulling of the PEG polymer network entangled wormlike micelles. In Fig. S3C, there is displayed a 3D-chip with a fully-surrounded 3D-focusing for the wormlike micelle solution with the same flow rate of v = 80 µL/h which leads to no jet-splitting effect anymore due to the missing wall contact of the wormlike micelles.

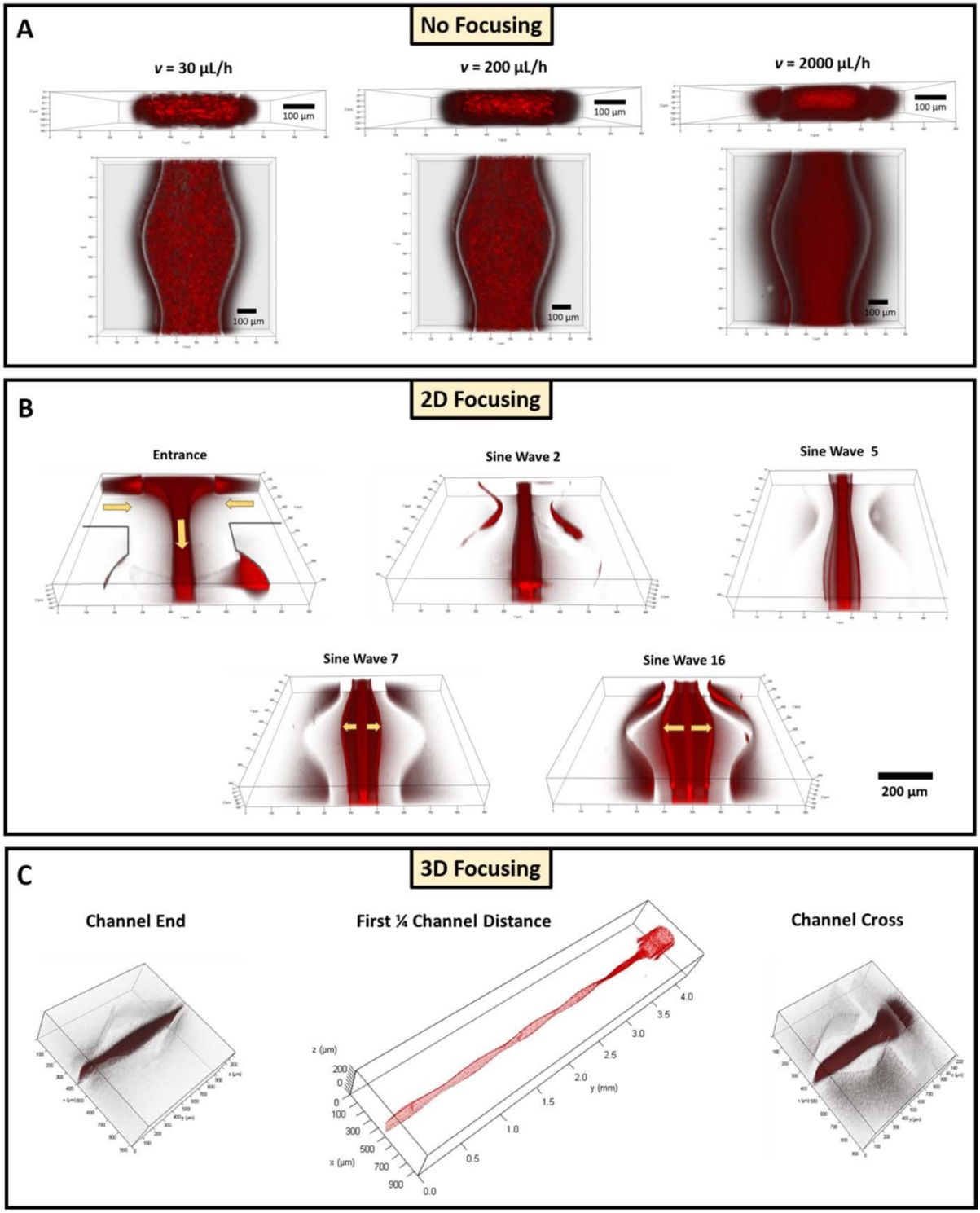

Fig. S3 3D-CLSM flow profile images of Nile red dyed wormlike micelles (1 wt%) within the standard sinusoidal microchannel (w = 250, P = 800, A = 150, h = 100, L = 15.000 µm). (A) 2D-chip with a mixture of 1 wt% wormlike micelles and 1 wt% PEG(900k) that is pumped with three various flow rates (v = 30 µL/h, 200 µL/h, 2000 µL/h) and without any focusing through one inlet channel whereby no jet-splitting effect appears. (B) 2D-chip with 2D-focusing of a wormlike micelles solution by two side channels via 1 wt% PEG(900k) that leads to rising jet-splitting within the sine channel. (C) 3D-chip with 3D-focusing of a wormlike micelle solution by two higher side channels does again not create a jet-splitting effect within the whole sinusoidal channel.

In following Fig. S4, there is shown a detailed analysis of the appeared jet-splitting effect of a 2D-laterally focused 1 wt% wormlike micelle solution with a flow rate of v = 200 µL/h for each of the three inlets of the sine channel (w = 250, P = 800, A = 150, h = 100, L = 15.000 µm) based on 3D-CLSM as well as polarization microscopy (PolMic) images. Fig. S4A illustrates the 3D-CLSM images with a front view of the flow profiles within the beginning cross section and after the third, seventh and ninth sinus wave along the sinusoidal microchannel. After the channel entrance, the jet-splitting starts directly at the cross section by existing extension rates and afterwards it increases within the first and all following sine waves due to further rising extension rates within each sine wave. It is clearly visible that the created sub-streams are pulled from the center towards the channel side walls just near to the channel top and bottom. Moreover, we can also observe that the two sub-streams are horizontally divided and forming four sub-streams which move subsequently after each sine wave more near to the channel edges. For each of the 3D-CLSM front view images also the matching polarized optical microscopy images from the top view are taken and displayed in Fig. S4B. PolMic makes it possible to analyze the flow orientation of the wormlike micelles within the microchannel. Here, the used quarter wave plate allows us to distinguish between an orange interference color for the vertically oriented micelles in flow direction and a blue color for the horizontally orientated micelles perpendicular to the flow. Consequently, all wormlike micelles within the main mid-stream are orientated in flow direction. The micelles within the two sub-streams are also quite orange and thus mainly aligned in flow direction but are able to turn out more within the sub-streams due to a lower flow velocity which is based on the parabolic flow profile conditions in a microfluidic channel.

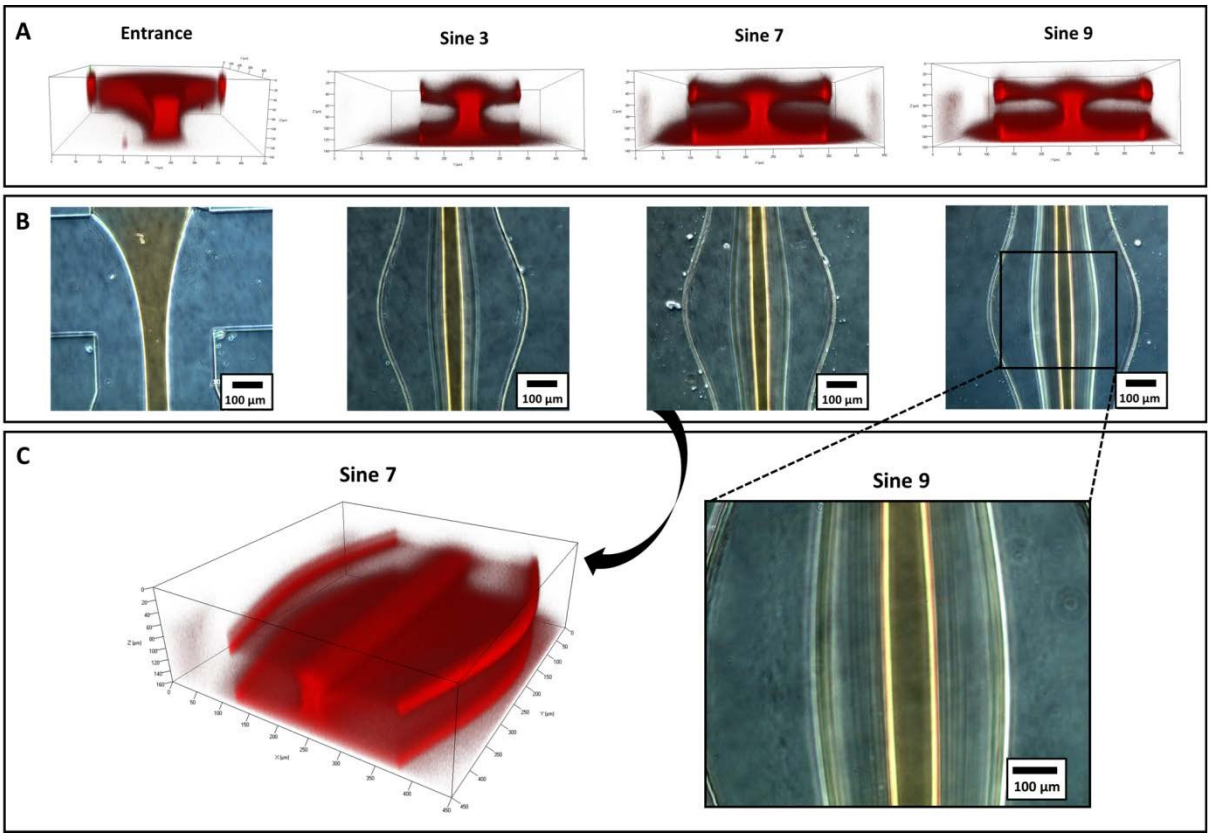

Fig. S4 (A) 3D-CLSM front view images of flow profiles from 1 wt% PEG (M = 900,000 g/mol) 2D-laterally focused Nile red dyed wormlike micelles (5 wt%) within the beginning cross section as well as after the third, seventh and ninth sinus wave along the sinusoidal microchannel. The flow rate amounts to v = 200 µL/h for all three inlets. (B) PolMic top view images to the upper 3D-CLSM images: Orange areas indicate orientation of wormlike micelles in flow direction y, and blue areas would indicate orientation in x axis which means perpendicular to the flow direction.

Moreover, flow profiles for different wormlike micelle concentrations are shown in ensuing polarization microscopy (PolMic) top view images of Fig. S5. The flow rates for each of the three channel inlets were again constant with v = 200 µL/h. The lowest focused wormlike micelle concentration of c = 1 wt% showed the broadest jet-splitting already at lower flow rates with less than v = 100 µL/h. With increasing concentration, up to c = 5 wt% the jet-splitting is visible just with higher flow rates more than v = 150 µL/h and the sub-streams can broaden up to the maximum which is limited by the channel side walls by using a flow rate of v = 1000 µL/h, shown in Fig. S5A. However, the jet-splitting does not occur anymore with the highest wormlike micelles concentration of c = 10 wt%, also for flow rates up to v = 500 µL/h as visible in Fig. S5B. The reason for the lower jet-splitting effect with higher wormlike micelles concentration is connected to the higher entanglement and thus viscosity. These properties make it more difficult for the PEG chains to pull the wormlike micelles out of center

position via the existing extensional rates within sinusoidal microchannels. Additionally, by using polarization microscopy it was also possible to analyze the flow orientation of the concentrated wormlike micelles within the channel. Here, the used quarter wave plate displays an orange interference color for the vertically oriented micelles in flow direction and a blue color for the horizontally orientated micelles perpendicular to the flow. Thus, all wormlike micelles are orientated in flow direction within the sub-streams and also the main mid-stream. Just for the 5 wt% micelles solution in Fig. 5SA a slight blue coloring of micelles orientated perpendicular to the flow direction is visible at the edge of the channel cross due to the lateral flow focusing.

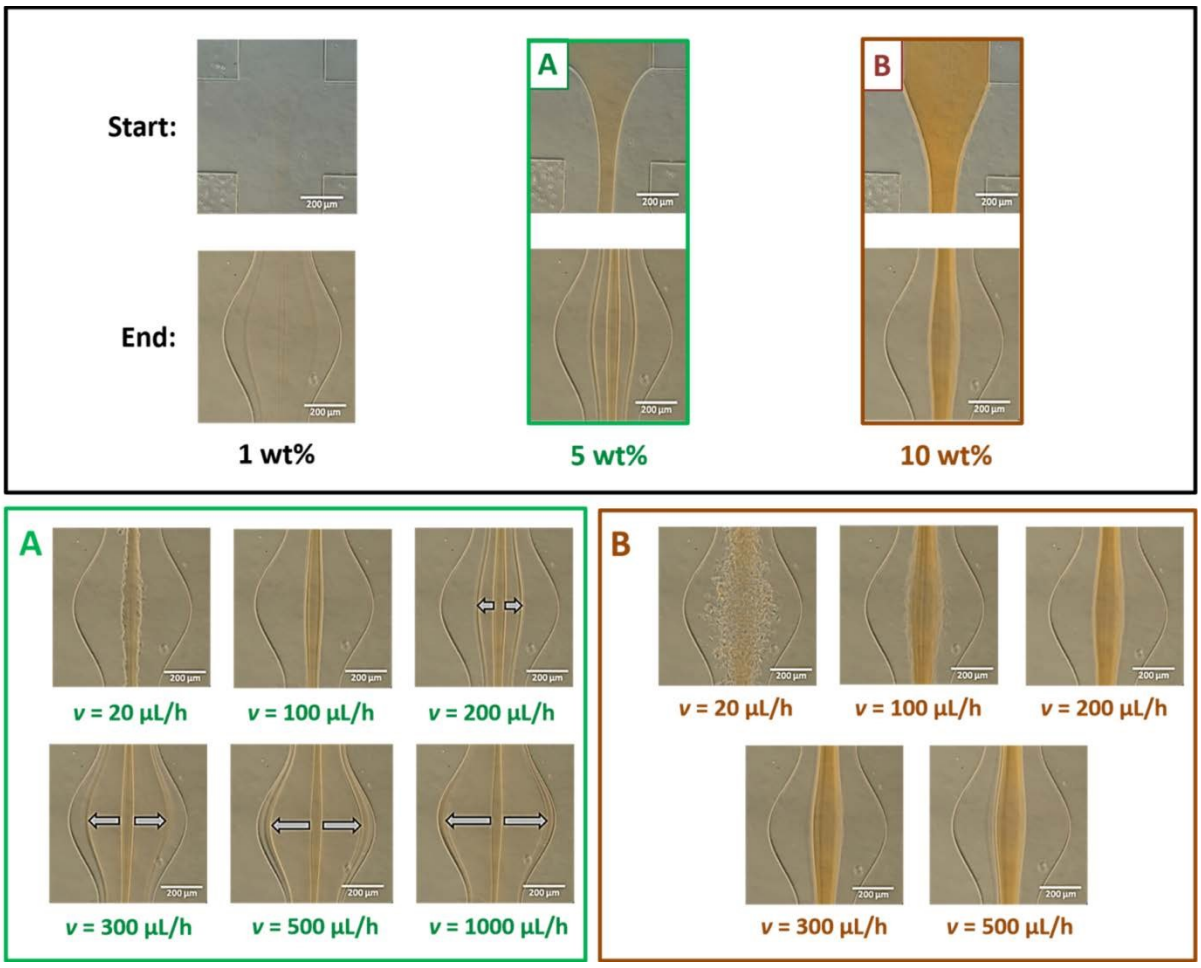

Fig. S5 Polarization microscopy (PolMic) top view images of flow profiles with a constant flow rate of $v = 200$ µL/h and three different wormlike micelles concentrations (1 wt%, 5 wt%, 10 wt%) again focused with 1 wt% PEG: (A) PolMic flow profiles of the 5 wt% wormlike micelles solution with varying flow rates between $v = 20$ µL/h and 1000 µL/h. (B) PolMic flow profiles of the 10 wt% wormlike micelles solution with varying flow rates between $v = 20$ µL/h and 500 µL/h.

Rheological Data

The rheological behaviour of the used focusing fluids was experimentally determined by a rheometer (Bohlin Germini HR^{Nano} Rotometic drive 2, Malvin Instruments GmbH). The rheometer was used in combination with a Peltier-plate (MV-4, JULABO USA Inc.) for temperature control and varying sizes of a coaxial cylinder-plate, cone-plate or plate-plate measurement system depending on the viscosity of the analyzed fluid. All measurements have been carried out with the rheometer software (Bohlin v2.0) by using a shear rate setting at a temperature of $T = 25$ °C. Fluids with a very low viscosity like water or the used 1 wt% PEG solution with a low molar mass of $M = 6{,}000$ g/mol was measured with the coaxial cylinder geometry C25 which has a diameter of $d = 25$ mm. For all other samples with much higher viscosity, like pure glycerin or 1 wt% PEG with a molar mass of $M = 300{,}000$ g/mol respectively 900,000 g/mol was measured with the cone-plate system CP4 /40 that has a diameter of $d = 40$ mm. All measured liquids which have been used as focusing fluids for the wormlike micelles respectively for the core-shell particles are visible in the rheological diagram of Fig. S5. Here, the Newtonian fluids, like the measured glycerin with a dynamic viscosity of $\eta = 956$ mPa·s or water with $\eta = 0.9$ mPa·s at $T = 25$ °C according to literature[2], show naturally constant viscosities with the tested shear rates from $\gamma = 1\text{E-}4\ s^{-1}$ up to $1.000\ s^{-1}$. These shear rates also include the shear rates which appear within a microfluidic channel. By evaluating the non-Newtonian solutions of 1 wt% PEG with different molar mass, a strong reduction of the viscosity is verified whereby the smallest viscosity for all three of them is always reached with a minimum shear rate of at least about $\gamma = 1\ s^{-1}$. All of these PEG's have an initial viscosity of about $\eta \approx 100{,}000$ mPa·s and with a shear rate higher than $\gamma = 1\ s^{-1}$ the viscosity for the PEG with a molar mass of $M = 900{,}000$ g/mol is decreased to a constant value of $\eta = 26$ mPa·s, respectively to $\eta = 12$ mPa·s for the PEG with $M = 300{,}000$ g/mol and to $\eta = 4$ mPa·s for the PEG with $M = 6{,}000$ g/mol. This evidenced shear thinning behavior here is the foundation for the explanation of the discovered jet-splitting effect and is based on the entangled polymer network of the non-Newtonian PEG focusing fluid which disconnects itself by the higher shear rates near to the channel walls[3].

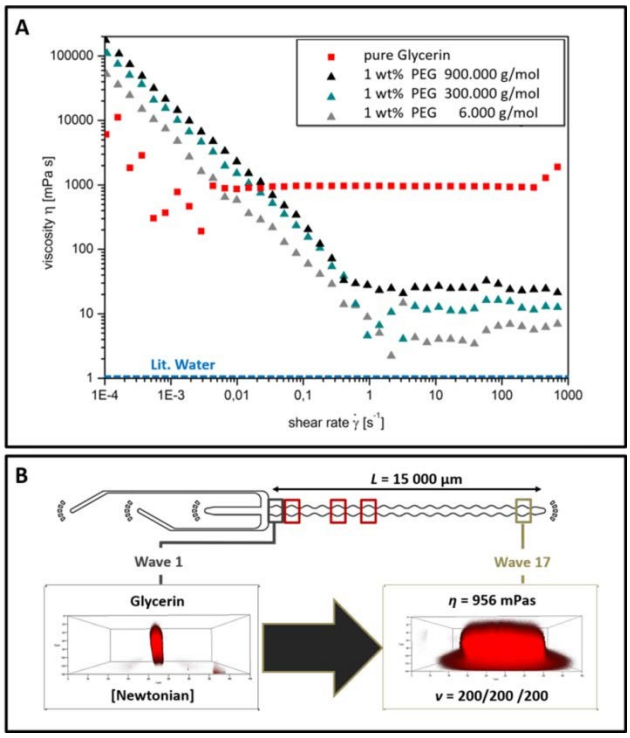

Fig. S6 (A) Rheological diagram about the viscosity curves of Newtonian glycerin, water and non-Newtonian 1 wt% PEG with different molar mass (M = 6,000 g/mol, 300,000 g/mol and 900,000 g/mol) in dependence from the shear rates. (B) 3D-CLSM front view images of the flow profiles of fluorescent dyed 1 wt% wormlike micelles in water within the standard sinusoidal channel (w = 250, P = 800, A = 150, h = 100, L = 15 mm) by using high-viscous Newtonian glycerin. The scatter of the data for glycerin at low shear rates and at shear rates >200 s^{-1} is due to limitations of the force sensor of the rheometer.

Separation and Purity

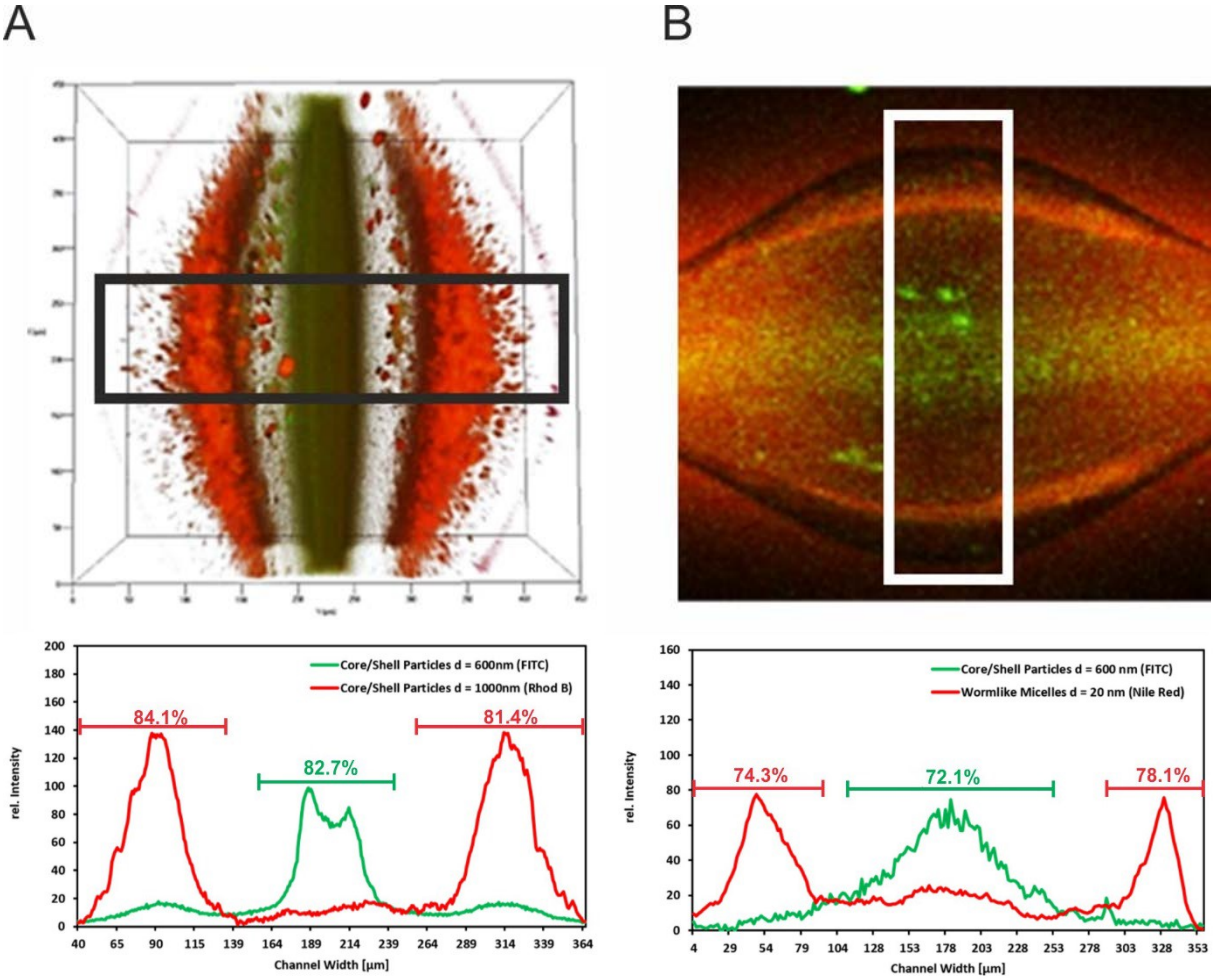

Fig. S7 (A) Section across the channel, indicated by the black rectangle (upper panel), with the corresponding fluorescence intensity profiles (lower panel), from which the purities for each of the separated 1000 nm SiO_2-PNIPAM core/shell particles (rhodamin-B-labelled, red) and 600 nm SiO_2-PNIPAM core/shell particles (fluorescein-labelled, green) was calculated. **(B)** Section across the channel, indicated by the white rectangle (upper panel), with the corresponding fluorescence intensity profiles (lower panel), from which the purities for each of the separated wormlike micelles (Nile red-labelled, red) and 600 nm SiO_2-PNIPAM core/shell particles (fluorescein-labelled, green) was determined. The scale bars indicate the integrated peak areas. The confocal images are reproduced from Fig. 4.

To calculate the purity of the sine channel-separated particles we chose the CLSM-images in Fig. 4 to quantitatively determine the fluorescence intensities for each of the particles across the channel as indicated in the regions of interest shown in Fig. S7. The background-subtracted fluorescence intensities shown in the lower panel of Fig. S7A show three peaks, two from the 1000 nm SiO_2-PNIPAM core/shell particles (rhodamin-B-labelled, red) in the outer streams, and one from the 600 nm SiO_2-PNIPAM core/shell particles (fluorescein-labelled, green) in the central stream. The purities were calculated

according to ref. [4] as $P_{1000} = \frac{A(red)}{A(red)+A(green)} 100\%$ for the 1000 nm core/shell particles, where *A(red)* and *A(green)* are the integrated intensities over the peaks in the outer streams, indicated by the red scale bars, and as $P_{600} = \frac{A(green)}{A(red)+A(green)} 100\%$ for the 600 nm core/shell particles, where *A(red)* and *A(green)* are the integrated intensities over the peak in the central stream, indicated by the green scale bar. We observe that after the 12th sine section there is a small fraction of 600 nm particles in the outer streams of the 1000 nm particles, and of 1000 nm particles in the central stream of the 600 nm particles. From the integrated peak areas we calculate purities of P_{1000} = 84 % for the 1000 nm particles in the left stream, and of 81% in the right stream. For the purity of the 600 nm particles in the central stream we obtain a value of 83%.

The background-subtracted fluorescence intensities shown in the lower panel of Fig. S7B similarly show three peaks, two from the wormlike micelles (Nile red-labelled, red) in the outer streams, and one from the 600 nm SiO_2-PNIPAM core/shell particles (fluorescein-labelled, green) in the central stream. The purities were similarly calculated as $P_{600} = \frac{A(red)}{A(red)+A(green)} 100\%$ for the wormlike micelles, where *A(red)* and *A(green)* are the integrated intensities over the peaks in the outer streams, indicated by the red scale bars, and as $P_{600} = \frac{A(green)}{A(red)+A(green)} 100\%$ for the 600 nm core/shell particles, where *A(red)* and *A(green)* are the integrated intensities over the peak in the central stream, indicated by the green scale bar. We observe that there is a small fraction of 600 nm particles in the outer streams of the wormlike micelles, and of wormlike micelles in the central stream of the 600 nm particles. From the integrated peak areas we calculate purities of P1000 = 74 % for the wormlike micelles in the left stream, and of 78% in the right stream. For the purity of the 600 nm particles in the central stream we obtain a value of 72%. Purities can be further increased by increasing the number of sine sections.

References

1 G. M. Whitesides and Y. Xia, *Annu. Rev. Mater. Sci.*, 1998, **28**, 153-184.

2 J. F. Coe and T. B. Godfrey, *Journal of Applied Physics*, 1944, **15**, 625-626.

3 M. Cross, *J Colloid Sci*, 1965, **20**, 417-437.

4 D. R. Gossett, W. M. Weaver, A. J. Mach, S. C. Hur, H. T. K. Tse, W. Lee, H. Amini, D. Di Carlo, *Anal. Bioanal. Chem*. 2010, **397**, 3249-3267.